Helmholtz resonant photoacoustic cell for spectroscopy of weakly absorbing gases and gas analysis

V.A. Kapitanov, V. Zeninari, D. Courtois, and Yu.N. Ponomarev

Institute of Atmospheric Optics,
Siberian Branch of the Russian Academy of Sciences, Tomsk, Russia
Champagne-Ardenne University, Reims, France

The results of experimental investigation into the design and geometry of resonant photoacoustic cells (Helmholtz resonator and differential Helmholtz resonator), as well as their sensitivity to gas pressure and modulation frequency of the exciting radiation are presented. A simple design of the Helmholtz resonator for flow measurements of absorption spectra and concentration of molecules is described. The characteristics of the resonant photoacoustic cells are theoretically analyzed based on the analogy with the electrical circuit approach. The test data for the designed photoacoustic cells with a CO_2 laser and near IR diode laser are presented.

1. Introduction

The laser photoacoustic spectroscopy due to its high sensitivity, wide dynamic range, and relatively simple realizability is at present a widely used method of designing spectroanalytical instruments for monitoring the atmospheric pollution. The detection threshold of photoacoustic (PA) instruments therewith is totally determined by the PA cell design and parameters of the laser source employed. The most popular sources are now high-power molecular gas lasers (CO_2 and CO lasers) and cw-tunable diode lasers. The optimum design of the PA cells should meet the following practical requirements[1,2]:

1. High sensitivity of a PA cell and high signal-to-noise (S/N) ratio;

2. Low rate adsorption (desorption) of the gas under study by the PA cell walls;

3. Feasibility of flow measurements (especially, in the case of high rate adsorption (desorption) by the cell walls);

4. Feasibility of measurements in noisy environment, e.g., close to traffic;

5. Feasibility of measurements under reduced pressure to increase the spectral selectivity and to decrease the interference of gases in multi-component mixtures[3];

6. Simple design and low cost.

When designing the PA cells which fulfill these requirements, the phenomenon of acoustic resonance in the cell chamber is widely used, e.g., excitation of longitudinal modes at single-path[3-5] or intracavity[6] irradiation of the PA cell; radial modes,[1,2] azimuthal modes in a windowless PA cell,[7] and so on. Almost all configurations of the PA cell have rather sophisticated design to provide suppression of ambient acoustic noise caused, for example, by gas flowing through the PA cell.[1,2] In this paper we discuss the applicability of the PA cell designed as the well-known acoustic Helmholtz resonator (HR).[8]
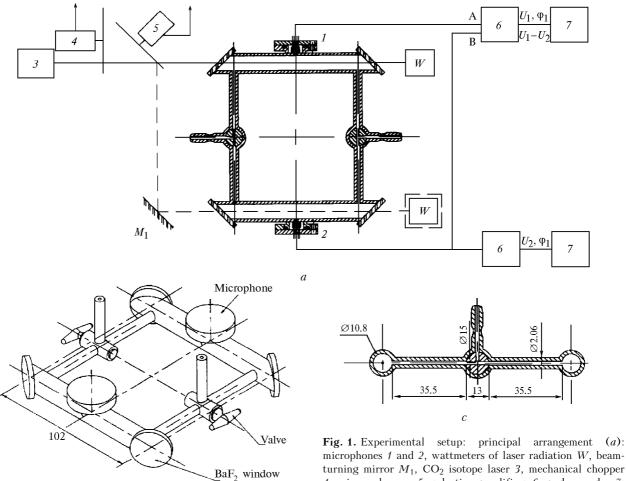
2. Helmholtz resonator

The Helmholtz resonator is simple in design and consists of two closed cell volumes (one equipped with a microphone) connected by a thin capillary tube. As compared to other acoustic resonators, the Helmholtz arrangement has the advantages of using cells of small volumes and low resonance frequency, which can be controlled by changing the dimensions of the capillary tube and cells. Besides, there is a possibility to enhance the S/N ratio using various differential schemes.

The Helmholtz resonance in PA cells was used for the first time in analysis of solid samples in order to separate the microphone cavity from the sample chamber.[8,9] An analysis of HR acoustic signals based on the equation for a driven harmonic oscillator[10] and acoustic analogy with the electrical circuit approach[11-13] describes both the HR responses as a function of frequency and values of the acoustic Q-factor with an acceptable accuracy. The differential Helmholtz resonator (DHR)[14] (with microphones in each of two identical cells and the difference between the microphone signals as a measured parameter) allows one to double the signal amplitude and to decrease significantly, at least by one or two orders of magnitude, the ambient noise. The double differential Helmholtz resonator (DDHR)[15] gives a possibility to eliminate the background signal.

In this paper we present the results of experimental investigation into sensitivities of PA nonresonant, HR, and DHR detectors as applied to detection of trace gases in the atmosphere, as well as theoretical analysis of sensitivities as functions of modulation frequency, cell pressure, and cell geometry. The theoretical analysis is based on the investigations reported in Refs. 16–21; in the experimental part of the paper we used the results from Refs. 11–13.

We also describe here a simple design of the Helmholtz resonator for flow measurements and an arrangement to double the photoacoustic signal of HR

Fig. 1. Experimental setup: principal arrangement (*a*): microphones *1* and *2*, wattmeters of laser radiation *W*, beam-turning mirror M_1, CO_2 isotope laser *3*, mechanical chopper *4*, mirror chopper *5*, selective amplifiers *6*, and recorder *7*; three-dimensional view of the PA cell (*b*); capillary tube (*c*).

or DHR. This is realized by replacing a standard chopper (black disk with holes) with a mirror chopper and by using the part of the laser energy, which otherwise is absorbed by the standard chopper, to irradiate the second cell of HR or DHR. The acoustic signals of such a PA system have been analyzed theoretically by acoustic analogy with the electrical circuit approach.[11–13]

Besides, the dependence of the HR and DHR photoacoustic detectors on gas pressure and additional volumes at flow measurements has been studied experimentally and theoretically.

3. Experiment

The experimental setup is shown in Fig. 1*a*. Radiation (ν = 1068.942 cm^{-1}, 9*P*20, power $\approx$ 1 W) of a continuous waveguide SAT C7 $O^{18}C^{12}O^{18}$ laser is chopped by a precision mechanical chopper (EG&G, model 197) at frequencies from 20 to 300 Hz. The laser beam is passed through the first cell of the PA detector made as DHR and then directed to the wattmeter. The radiation wavelength is checked by the CO_2 spectrum analyzer (Optical Engineering).

In order to double the acoustic signal of the HR and DHR photoacoustic detectors, we replaced the mechanical chopper with a mirror chopper with a gold coated sector disk and used 100% reflectivity mirror M_1 to direct the opposite in phase (relative to the first cell) modulated laser radiation into the second cell of the detector.

To investigate the parameters of nonresonant, HR, and DHR detectors and the feasibility of flow measurements, our photoacoustic detector (Fig. 1*b*) was built as two identical glass PA cells. Each cell was equipped with a low-cost commercial electret Knowles EK3024 microphone and BaF_2 windows mounted at the Brewster angle. The cells were connected to each other by two identical Pyrex capillary tubes with three-way vacuum valves (Fig. 1*c*) to form a bilateral symmetric design. The three-way valves allowed us to change the PA configuration and to investigate each nonresonant detector separately or HR and DHR photoacoustic detectors with one or two capillary tubes, as well as to carry out flow measurements.

Parameters of the PA detectors (sensitivity as a function of frequency, pressure, and type of the buffer gas) in various configurations were studied

using mixtures of ethylene in the vapor phase (the closest absorption line $\nu = 1068.9959$ cm^{-1}, $S = 8.42 \cdot 10^{-21}$ cm^{-1}·molecules·cm^2) as an absorbing gas and N_2 as a buffer gas. The mixtures were prepared in a laboratory vacuum tank. The AW 1000 mbar Effa manometer was used to measure the gas pressure. The mixtures were kept for 3 or 4 hours before measurements. We used mixtures with rather high concentration of C_2H_4 to measure the absorption coefficients at the laser wavelength. The amplitudes and phases of the PA signals U_0, U_1, U_2, $U_1 - U_2$, φ_1, and φ_2, as functions of frequency were measured by two lock-in-amplifiers (EG&G, model 5301, $t = 1$ s, and $Q = 20$).

4. Theoretical analysis of sensitivity of the nonresonant detector

The analytical potentialities of PA detectors are completely determined by such important characteristics[23] as sensitivity R, V·W^{-1}·m, and threshold sensitivity $\Lambda = \sqrt{u_n^2}/R$ in (W·m^{-1}·Hz$^{-1/2}$), where $\sqrt{u_n^2}$ is the root-mean-square value of noise in the recording system, in V·Hz$^{-1/2}$, reduced to the corresponding value at the preamplifier input. In the case of weakly absorbing media ($K_v \cdot l_C \ll 1$, where K_v is the absorption coefficient, in m^{-1}, and l_C is the cell length, in m) and absence of saturation effects, the sensitivity R characterizes the efficiency of transformation of the absorbed power into the output electrical signal of the acoustic sensor[21]; it is the amplitude of the electrical signal produced by the sensor per unit power absorbed by the investigated medium of unit length. The threshold sensitivity Λ is a minimum absorbed power per unit length detectable by the photoacoustic detector given the S/N ratio (usually it is taken S/N = 1), frequency, and frequency band. Highly sensitive electrostatic microphones are widely used for measuring pressure oscillations. In this case the sensitivity of the photoacoustic detectors can be presented as the product of microphone sensitivity R_m, in V·Pa^{-1}, and cell sensitivity $R_C = \Delta P/W_0 K_v$, where ΔP (in Pa) is the rms increase of the gas pressure in the cell, and W_0 (in W) is the power of the radiation source. In the proposed presentation this characteristic is independent of the source power and the absorption coefficient of the gas under study, but depends on the dimensions of the cell, microphone sensitivity, thermodynamic parameters of the gaseous medium macrocomposition (the most important and variable of them are the pressure and temperature), and the properties of molecules under study.

Despite a lot of papers dedicated to analysis of generation of pressure signals and modifications of PA cells, the dependence of their sensitivity on thermodynamic parameters of the medium, in particular, pressure are poorly studied. Only such parameters of gas as thermal capacity and thermal conductivity are commonly taken into account.

Amplitudes of pressure oscillations ΔP due to interaction of the modulated radiation with the absorbing gaseous medium in a closed volume of the photoacoustic detector are determined by the following processes:

1. Change in population of the energy levels falling in resonance with the radiation frequency;

2. Transformation of the energy of molecules excited by the laser radiation to thermal energy of the gas in the process of their relaxation to the initial state;

3. Temperature and pressure oscillations of the gas in the chamber volume.

The gas pressure oscillations ΔP of the PA detector and, correspondingly, sensitivities R_C of nonresonant and resonant cells were analyzed for the case of coherent sources in Refs. 16–21, and 27. Kerr and Atwood[16] have obtained the expression for the mean increase in pressure ΔP generated in a long tubular cell ($l_C \gg a$, where a, in m, is the cell radius) at absorption of the radiation modulated by rectangular function with the frequency $\omega \ll \tau_T^{-1}$. They also have determined such principal parameter of the photoacoustic detector as the time of thermal relaxation in the cell $\tau_T = a^2/5.76\,k$, where k (in m^2·s^{-1}) is the gas thermal diffusivity. Then these results were used to measure the nitrogen and argon thermal diffusivity at the temperature equal to 293 K (Ref. 28) and ranging from 290 to 423 K (Ref. 29); they used the expression $\tau_T = a^2/6.046\,k$ to determine k. Kreuzer[17] analyzed the energy relaxation of the vibrationally excited molecules to the translational energy at the sine modulation of the intensity with small modulation depth ($\delta \ll 1$) as well as background signals, Brownian noise of the microphone membrane, and Johnson noise. He used the equation $\tau_T = C_V \cdot a^2/(40 \cdot K)$ for the thermal relaxation time, where $C_V = c_V \cdot \rho$ is the heat capacity (in J·K^{-1}) and K is the thermal conductivity (in W·m^{-1}·K^{-1}). References 18–20 present the model describing the pressure oscillations in the cell of the photoacoustic detector due to absorption of the trapezoidal wave modulated beam and analyze the detection limits for concentrations of some impurities. The effect of energy relaxation of the vibrationally excited molecules due to collisions with the cell walls and the PA detector sensitivity at the reduced pressure were considered in Ref. 21.

If the radiation intensity is modulated with a mechanical chopper, the time dependence of the intensity is of trapezoidal shape and the rms increase of pressure $\Delta P(\omega)$ at the first harmonic can be presented as[18,20]

$$\Delta P(\omega) =$$

$$= \frac{2^{1/2}(\gamma - 1)\, d\, W_0\, K_v\, l_C\, Q(\omega)\, \tau_T}{\pi V \tau_C (\tau_C^{-1} + \tau_R^{-1})[1 + (\omega \tau_T)^2]^{1/2}\{1 + [\omega(\tau_C^{-1} + \tau_R^{-1})^{-1}]^2\}^{1/2}},$$

$$(1)$$

where γ is the isentropic exponent, $d = \sin(t_r/T_\omega)\times(t_r/T_\omega)^{-1}$ is the coefficient characterizing the deviation of a trapezoidal wave function from a square wave function (t_r and T_ω are the time of increase and the period of the trapezoidal function, respectively), $Q(\omega)$ is the acoustic Q-factor of the PA cell, $V = \pi a^2 l_C$ is the cell volume, τ_C (s) is the vibrational–translational relaxation time, t_R (s) is the radiative relaxation time: in the case if the mean power W_m is measured at the cell output, $W_0 = 2W_m/\theta$, where θ is the transmittance of the cell window. The factor $[\tau_C(\tau_C^{-1} + \tau_R^{-1})]^{-1}$ in Eq. (1) determines the portion of the absorbed energy, which is transformed into pressure oscillations and the thermal energy of the medium under study. The character of the dependence $\Delta P(\omega)$ on thermodynamic parameters of the medium macrocomposition and the molecular properties is determined by the relations between the energy relaxation rates of excited molecules, thermal relaxation of the cell, and modulation frequency.

At reduced pressure the energy relaxation of excited molecules on the cell walls (or heterogeneous relaxation) becomes important,[21,27] and the resulting relaxation rate τ_S^{-1} is determined as

$$\tau_S^{-1} = \tau_R^{-1} + \tau_C^{-1} + \tau_{\text{het}}^{-1}. \qquad (2)$$

The energy relaxation rates of excited molecules (except for the radiative rate) depend on the cell pressure P (in Pa). The time of vibrational–translational, heterogeneous, and thermal relaxation as a function of pressure can be written as

$$\tau_C = \tau_C^0/P; \quad \tau_{\text{het}} = \tau_{\text{het}}^0 P; \quad \tau_T = \tau_T^0 P, \qquad (3)$$

where τ_C^0, τ_{het}^0, and τ_T^0 are the corresponding relaxation times reduced to the unit pressure (in s·Pa, s·Pa^{-1}, and s·Pa^{-1}). The values of the relaxation times for most molecules in the visible and IR spectral ranges at the atmospheric pressure are within the following limits $\tau_R \cong 10^{-0} - 10^{-2}$ s, $\tau_C \cong 10^{-4} - 10^{-7}$ s, and τ_{het}, $\tau_T \cong 10^{-1} - 10^{-3}$ s and, as a rule, the conditions

$$\tau_R^{-1} \ll (\tau_C^{-1} + \tau_{\text{het}}^{-1}); \quad \tau_C^{-1} \gg \tau_T^{-1} \qquad (4)$$

hold true in a rather wide range of pressures ($10^3 - 10^5$ Pa). Using Eqs. (2) and (3) in the rate equations for the upper-state population[17] and taking into account all the above mentioned, the sensitivity R_C as a function of the frequency and pressure can be written as:

$$R_C = \frac{2\Delta P(\omega)}{\theta\, W_m\, K_\nu} = \frac{1}{1.11\cdot\theta\pi a^2} \times$$

$$\times \frac{(\gamma - 1)\, Q(\omega)\, (\tau_{\text{het}}^0/\tau_C^0)\, P^2\, \tau_T^0\, P}{\left(1 + \frac{\tau_{\text{het}}^0}{\tau_C^0}P^2\right)(1 + (\omega\tau_T^0)^2 P^2)^{1/2}\left[1 + \omega^2\left(\frac{\tau_{\text{het}}^0 P}{1 + \tau_{\text{het}}^0 P^2/\tau_C^0}\right)^2\right]^{1/2}}. \qquad (5)$$

The heterogeneous relaxation time τ_{het} depends on the time of diffusion of excited molecules to the cell walls and can be estimated[21,27,30] from

$$\tau_{\text{het}} = \varepsilon\frac{a^2}{5.76D} \cong \varepsilon\tau_T; \quad D \cong \frac{K}{\rho c_V}, \qquad (6)$$

where ε is the accommodation coefficient (the probability of energy relaxation of an excited molecule at collision with the cell wall $\varepsilon \cong 1$), D (in m^2·s^{-1}) is the diffusion coefficient, and ρ (in kg·m^{-3}) is the gas density.

For nonresonant cells, in Eq. (5) the acoustic Q-factor $Q(\omega) = 1$ (Ref. 20), $\tau_T = a^2/(6.047k) = a^2\rho c_V/(6.047K)$ (Refs. 28 and 29), and $\rho c_V = P/(\gamma - 1)T$; and for pressures and frequencies whose modulations

$$\varepsilon\tau_T^0\, P^2/\tau_C^0 \gg 1 \qquad (7)$$

and

$$\omega \ll (\tau_T^0\, P)^{-1}, \qquad (8)$$
$$\omega \ll (\tau_C^0\, P)^{-1}, \qquad (9)$$

the sensitivity of the nonresonant cell R_{C0} is independent of the frequency and inversely proportional to the pressure[16]

$$R_{C0} = P/(6.716\pi KT\theta), \qquad (10)$$

where T is the gas temperature in the cell.

At low pressure ($\varepsilon\tau_T^0\, P^2/\tau_C^0 \ll 1$ and $\lambda \cong a$, where λ is the mean free path) the thermal conductivity is in directly proportional dependence with the pressure: $K \cong K'P$ and the cell sensitivity is[21,27]:

$$R_{C0} = \varepsilon\tau_T^0\, P^2/(\tau_C^0\, 6.716\pi K'T\theta). \qquad (11)$$

At sufficiently high modulation frequency

$$(\tau_T^0\, P)^{-1} \ll \omega \ll (\tau_C^0\, P)^{-1} \qquad (12)$$

the sensitivity

$$R_{C0} = (\gamma - 1)/(1.11\theta\pi a^2\omega), \qquad (13)$$

is independent of the pressure, inversely proportional to the modulation frequency and the squared cell radius, and dependent on the isentropic exponent of the principal gas filling the cell.[17,27]

However, at low pressure, high frequency, and large vibrational–translational relaxation time of absorbing molecules ($(\tau_C^0\, P)^2 \geq 1$), the sensitivity

$$R_{C0} = \frac{(\gamma - 1)}{1.11\theta\pi a^2\omega\,[1 + (\omega\tau_C^0/P)^2]^{1/2}} \qquad (14)$$

becomes pressure dependent at rather high modulation frequency $R_{C0} \approx \omega^{-2}$. This change in the character of frequency dependence of the sensitivity may be used to determine the vibrational–translational relaxation times of molecules.[33] Note that depending on the cell pressure and relaxation times, the character of the
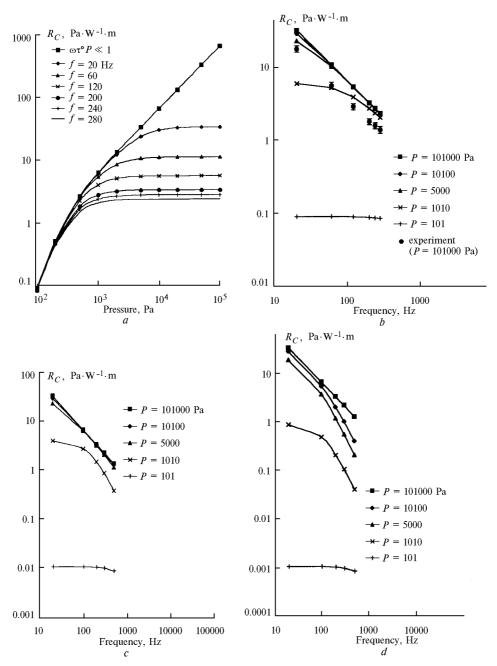
Fig. 2. Sensitivity of the PA cell vs. gas pressure (*a*) and modulation frequency (*b*, *c*, and *d*). In calculation by Eq. (5) the following values were used: $\tau_C = 10^{-6}$ (*a*, *b*), 10^{-5} (*c*), and 10^{-4} s (*d*).

frequency dependence of the sensitivity (Fig. 2) varies from frequency independent to $R_{C0} \approx \omega^{-2}$, what explains the results obtained in Refs. 19, 21, and 31. In the region of low pressures, where vibrational–translational relaxation competes with deactivation of excited molecules on the PA cell walls, the behavior of the pressure dependence of R_{C0} at constant frequency (Fig. 3) substantially depends on τ_C. This fact was successfully used in measurements of the vibrational–translational relaxation times.[21]

The sensitivity of the nonresonant PA cell calculated by Eq. (5) as a function of the frequency and gas

(nitrogen) pressure is shown in Figs. 2 and 3. In the calculations we have used the values of the physical constants[22] (see the Table 1) and $\theta = 0.95$; $(\gamma - 1) = 0.4$;

$$a = 5.4 \cdot 10^{-3} \text{ m}; \quad Q(\omega) = 1; \quad \tau_T^0 = \frac{a^2}{6.047 k_{N_2} 1.01 \cdot 10^5} \text{ Pa}^{-1} \cdot \text{s};$$

$$\tau_{\text{het}}^0 = \varepsilon \tau_T^0 \cong \tau_T^0 = 1.59 \cdot 10^{-6} \text{ Pa}^{-1} \cdot \text{s}; \quad \text{and} \quad \tau_C^0 = \tau_C \cdot 1.01 \cdot 10^5 \cong \cong 10^{-1} \text{ Pa} \cdot \text{s}.$$

At the atmospheric pressure the PA signal ΔP and the sensitivity of the nonresonant cell R_{C0} are proportional to ω^{-1} (see Fig. 2*b*) at the pressure and vibrational–translational relaxation time varying within a wide range.
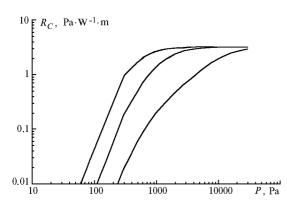
V.A. Kapitanov et al.

Vol. 12, No. 10 /October 1999/ Atmos. Oceanic Opt.   933

Fig. 3. Cell sensitivity vs. gas pressure in it at different values of τ_C: 10^{-6} (*1*), 10^{-5} (*2*), and 10^{-4} s (*3*). Modulation frequency is 200 Hz.

Table 1. Characteristics of gases, acoustic cell, and electrical circuits used in calculations

Parameters	C_2H_4	N_2
Thermal conductivity K, W $/$ (m·K)		$2.598 \cdot 10^{-2}$
Thermal diffusivity k, m^2/s		$0.3 \cdot 10^{-4}$
$C_p/C_V = \gamma$		1.4
Specific heat capacity C_V, J $/$ (kg·K)		718
Collisional relaxation time τ_C, s	10^{-6}	
Sonic speed v_s, m$/$s	329 (Ref. 22)	346 (Ref. 22)
Mass density ρ, kg$/$m^3	1.1746 (Ref. 22)	1.1662 (Ref. 22)
Viscosity η, m^{-1}·kg·s^{-1}	$1.04 \cdot 10^{-5}$ (Ref. 22)	$1.79 \cdot 10^{-5}$ (Ref. 22)
Equivalent capacity $C_{1,2}$, m^4·s^2·kg^{-1}	$7.55 \cdot 10^{-11}$	$6.88 \cdot 10^{-11}$
Equivalent resistance R, kg·m^{-4}·s^{-1}	$6.30 \cdot 10^6$	$8.79 \cdot 10^6$
Equivalent inductance L, kg·m^{-4}	33663	33422
Resonance frequency, Hz	200	210

5. Method of electroacoustic analogy

The most feasible and simple way to analyze the PA signals caused by absorption of the modulated radiation in resonant cells is the method of electroacoustic analogy[34,11–13] based on the similarity of differential equations describing the states of acoustic systems and electrical circuits. Based on comparison of the similar equations, the Table 1 of acoustic and electrical analogs is drawn. If the wavelength of acoustic waves exceeds the dimensions of the acoustic system, the equivalent electrical circuit is represented by discrete circuit elements; and in the table of analogs the amplitude of voltage U oscillations corresponds to the amplitude of pressure oscillations (in Pa), the electrical current I corresponds to the volume rate (in m^3·s^{-1}), the inductance L corresponds to the acoustic mass (in kg·m^{-4}), the capacitance C corresponds to the acoustic capacitance (in m^4·s^2·kg^{-1}), and the resistance R corresponds to the acoustic resistance (kg·m^{-4}·s^{-1}).

The energy sources of the PA effect causing harmonic oscillations in a nonresonant PA cell are absorption of modulated radiation and the following transformation of the absorbed energy into heat. If, according to the table of analogs, the pressure oscillations ΔP corresponds to the voltage oscillations U_c across the capacitance, then the heat source is equivalent to the source of alternating current $I_0 = I_0 \sin \omega t$ (the source of emf with high intrinsic resistance R_{in}), because according to Eqs. (1) and (13) and the definition of sensitivity (under fulfillment of condition (12)), the amplitude and phase of pressure oscillations in the nonresonant cell

$$\Delta P_0 = \frac{(\gamma - 1) \, W_0 \, K_v}{1.11 \pi a^2 \omega} \sin(\omega t - \varphi), \qquad (15)$$

$$\varphi = - \arctan \omega \tau_T \qquad (16)$$

depend on the frequency in the same manner as the amplitude and phase of voltage across the capacitance of the equivalent electrical circuit (Fig. *4b*)

$$U_0 = I_0 \sin(\omega t - \varphi)/(C\omega), \qquad (17)$$

$$\varphi = - \arctan \omega R_{in} \, C. \qquad (18)$$

On the assumption that the acoustic wavelength significantly exceeds the dimensions of the PA cells, the equivalent capacitance C_i, active resistance R, and inductance L of the HR consisting of two equal volumes V_i connected by capillary tubes of length l and radius r (the air mass in the capillary tubes oscillates between the volumes with the frequency of modulation) is determined as[11–13]

$$R_i = \frac{8\rho l \omega}{(\pi r)^3} (d_v + (\gamma - 1)d_t); \quad L_1 = \frac{\rho l}{\pi r^2}; \quad C_i = \frac{V_i}{v_s^2 \rho}, \quad (19)$$

where v_s is the sonic speed, and ρ is the density of the gas in the cell. Thicknesses d_v and d_t of the viscosity and thermal boundary layers near the walls of the capillary tubes are determined from

$$d_v = \sqrt{2\eta/(\rho\omega)} \text{ and } d_t = \sqrt{2K/(\rho\omega c_p)}, \qquad (20)$$

where η is the dynamic viscosity (in m^{-1}·kg·s^{-1}), K is the thermal conductivity, and c_p is the specific heat at constant pressure (in J·kg^{-1}·K^{-1}). Taking into account Eqs. (15), (17), and (19), the equivalent amplitude of the current I_0 oscillations can be expressed as

$$I_0 = (\gamma - 1) \, W_0 \, K_v \, l_C/(1.11\rho v_s^2). \qquad (21)$$

The equivalent values of R_1 and L_1 are determined only by the size of the capillary tube and molecular parameters of the gas in the PA cell. So, in the calculations, the design features of the capillary tube were taken into account (Fig. *1c*). In Fig. 1 R_1 and L_1 are series connections of resistors and inductors corresponding to various parts of the capillary tube. The values of the capacitances C_i depend on the volume of both the cells and capillary tubes, and for our

configuration of HR $V_1 = V_2 = (\pi a^2 l_C + \pi r^2 l)$. The presented configuration of the PA cell allows formation of photoacoustic detectors (PAD) of various types: nonresonant detectors, HR, DHR with one or two capillary tubes, DHR for flow measurements, as well as the use of standard or mirror choppers for radiation modulation (Fig. 4).

As noted above, the capacitor microphones are widely used for recording pressure oscillations in the PAD cell. Their sensitivity R_m strongly depends on the frequency[32] (this is especially true for the microphones operating in the frequency range from 20 to 300 Hz we used in our experiments) and pressure.[21] The microphones introduce uncontrollable phase shift, which also depends on the frequency and pressure. Besides, the amplitude and phase of current oscillations I_0 (21) depend on the same parameters as

well. In order to eliminate the influence of the microphones and the PA effect inside the nonresonant cell and to study the resonance properties of the HR and DHR themselves, correction of their PA signals $U_1(\omega)$, $U_2(\omega)$ and phases $\varphi_1(\omega)$, $\varphi_2(\omega)$ by signals $U_0(\omega)$ and phases $\varphi_0(\omega)$ of the nonresonant PAD is required.

Within the framework of the method of electroacoustic analogy, the frequency dependence of the normalized amplitudes $U_1(\omega)/U_0(\omega)$; $U_2(\omega)/U_0(\omega)$; $(U_1(\omega) - U_2(\omega))/U_0(\omega)$ and relative phase shifts $\varphi_1(\omega) - \varphi_0(\omega)$; $\varphi_0(\omega) - \varphi_2(\omega)$; $\varphi_1(\omega) - \varphi_2(\omega)$ of PA signals were directly calculated. To do this, we have used the equations from Ref. 12 and MicroSim Pspice Analog/Digital Simulation and MicroSim Schematics (MicroSim corporation, California, USA) Version 6.3.
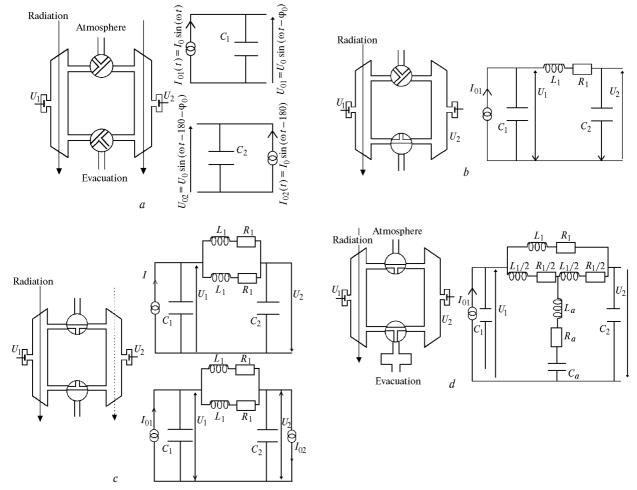

Fig. 4. Schematic representation of the PA detectors and their equivalent electrical circuits: the scheme of two-chamber nonresonant PA cell (the second cell is irradiated in antiphase relative to the first one) and equivalent electrical circuits of these cells. Generation of an acoustic signal due to the PA effect and the response of the microphones correspond to a source of alternating current I_0 and voltage U_{0i} (*a*); optical and equivalent electrical circuit of two PA cells connected with one capillary tube (*b*); optical and equivalent electrical circuit of two PA cells connected with two identical capillary tubes. The dashed line shows the additional exposure of the second cell to the modulated radiation in antiphase with the use of a mirror chopper. The top circuit corresponds to the case of modulation with the mechanical chopper, the lower one is for the case of the mirror chopper (*c*); optical and equivalent electrical circuit of the open PA cell for flow measurements. Additional volumes are coupled to the PA detector. The additional volume is a thin (6 mm in diameter, 1.1 m in length) vacuum tube ($V = 30 \cdot 10^{-6}$ m^3, $C = 220$ pF). The additional capillary tube is equal to about a half of the capillary tube connecting the PA cells ($L_a = 14400$ H, $R_a = 3.9 \cdot 10^6$ λ).

6. Results and discussion

6.1. Sensitivity of nonresonant PA cell

Frequency dependence of the sensitivity R at cell pressures of 1000, 500, and 100 mbar is shown in Fig. 5a. The values of the sensitivity R ($P = 1000$ mbar) were obtained from measuring concentration characteristics at each fixed frequency using the mixtures of ethylene with N_2 at the C_2H_4 partial pressure of 0.3, 3, 10, 15, 80, and 125 mbar. The concentration characteristic at 200 Hz frequency is exemplified in Fig. 6. The PA signal normalized to the source power linearly depends on the concentration within the range covering almost four orders of magnitude. Nonlinearity at low concentrations ($0.3 \cdot 10^{-4}$) is stipulated by a large background signal (PA signal due to absorption by cell windows and walls), which is among the main limiting factors determining the threshold concentration sensitivity in the PA systems with CO_2 lasers.[1,2] In the absence of radiation the measured rms level of noise at the microphone output was about 1 μV. When the cell filled with pure N_2 was exposed to the modulated radiation at the frequency of 200 Hz, the value of the signal/power ratio was 0.160 mV·W^{-1}, i.e., two orders of magnitude higher than the noise level. The absorption coefficient of ethylene at the laser wavelength ($v_L = 1068.9425$ cm^{-1}) was determined from measurements of the PA cell transmission at high concentrations of ethylene ($K_v = (0.21 \pm 0.02)$ cm^{-1}·atm^{-1}). The frequency dependence of the sensitivity R strongly differs from the linear one, and to determine $R_{C0} = R/R_m$, we used the typical response of the Knoweles EK3024 microphone[32] (Fig. 5b). The frequency dependence $R_{C0} \approx f^{-1}$, where $f = \omega/2\pi$, is shown in Fig. 2b as compared to that calculated by Eq. (5). The difference between the experimental and calculated values is likely connected with variations of the microphone sensitivity (± 3 dB) (Ref. 32).

The sensitivity R at the reduced pressure of 100 mbar was studied using pure ethylene because it was needed to measure the absorption coefficient, and then ethylene was diluted with N_2 to the pressure of 500 mbar. The obtained values of the coefficients were $K_v = (0.009 \pm 0.001)$ and (0.019 ± 0.002) cm^{-1}, respectively. The values of R at the reduced pressure and those at the atmospheric pressure differ significantly. As shown in Ref. 21, R_m strongly depends on pressure and grows with its decrease. Taking into account that under fulfillment of condition (12) R_{C0} is independent of pressure (Eq. (13)) and adiabatic curves of N_2 and ethylene differ insignificantly, the experimentally obtained values of R were used to find the frequency characteristics of the Knoweles EK3024 microphone at reduced pressure (Fig. 5b). The presented results show that R_m strongly depends on pressure and increases as it falls. Unfortunately, we failed to measure the phase shift of PA signals because of uncontrollable phase shift introduced by the microphone.
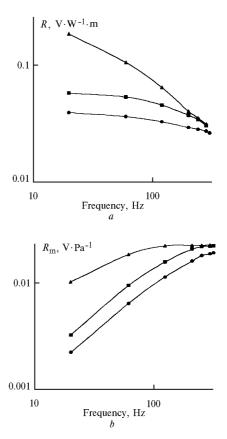

Fig. 5. PAD sensitivity (a) and microphone sensitivity (b) vs. the modulation frequency of radiation at various gas pressure in the cell: 0.1 (triangles), 0.5 (squares), and 1 atm (circles). The microphone sensitivity at low pressures was found from the equation $R_m(\omega) = R(\omega)/R_C(\omega)$, where R_C is independent of pressure.
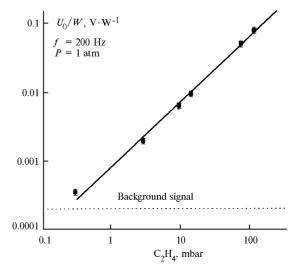

Fig. 6. Concentration characteristic curve of nonresonant PA detector. Modulation frequency is 200 Hz; pressure in the cell is 1 atm.

The experimentally measured and calculated R values are shown relative to the mean power of the modulated radiation. To obtain the data on the source power, these values should be halved.

6.2. Frequency characteristics of HR and DHR PA detectors

As mentioned above, to eliminate the effect of frequency characteristics of the nonresonant cell and microphone, as well as to separate out the frequency characteristics of the HRs themselves, it is necessary to measure the ratios of the signals of resonant and nonresonant PADs and their phase shifts. So, we measured the PA signals of PA detectors of all types (nonresonant, HR, DHR with one and two capillary tubes, with standard and mirror choppers) at each frequency simultaneously using the ability of our PA system to readily change its configuration. First, for each frequency the PA signal U_0 and phase φ_0 of the nonresonant detector were measured, then the PA cell configuration was rebuilt into the one-capillary HR configuration and then into two-capillary DHR configuration. For each configuration the PA signals U_1 and U_0, phases φ_1 and φ_2 (HR configuration), $(U_1 - U_2)$ (DHR configuration) were measured and then the ratios $A_1 = U_1/U_2$, $A_2 = U_2/U_0$, and $A_{12} = (U_1 - U_2)/U_0$ as well as the phase shifts $(\varphi_1 - \varphi_0)$, $(\varphi_0 - \varphi_2)$, and $(\varphi_1 - \varphi_2)$ were calculated.

The experimentally obtained values of the frequency characteristics of the ratios A_1, A_2, A_{12}, and phase shifts for the HR and DHR configurations with one and two capillary tubes (Fig. 7) are described by the calculated frequency characteristics of the equivalent electrical circuits (Fig. 4) with the experimental accuracy.

The parameters of gaseous media[22] and the corresponding calculated values of parameters of equivalent electrical circuits with regard for the design features of the capillary tubes are given in the Table 2. By definition, the sensitivity of the resonant PAD may be presented as

$$R = U_1/(K_v\ W_0) = A_i\ R_0 \qquad (22)$$

as opposed to the definition given in Refs. 13, 18–20 and used in Eq. (5).

The experimental and theoretical values of the acoustic Q-factor $Q_i = \omega_{0i}/\Delta\omega_i$ for various HRs are about twice as large as the corresponding ratios A_i, therefore Eq. (22) should be used for determining the HR and DHR sensitivity.

To check the HR and DHR models based on the electroacoustic analogy and Eqs. (19) and (20) describing the equivalent electrical parameters, we measured the HR and DHR frequency characteristics with pure ethylene at the atmospheric pressure. Physical constants of ethylene differ from those of N_2: the sonic speed and density are almost the same, but the ethylene viscosity is about 1.7 times less than that of N_2. The equivalent scheme (Fig. 4) allows calculating the HR and DHR frequency characteristics with the experimental accuracy (Fig. 8).
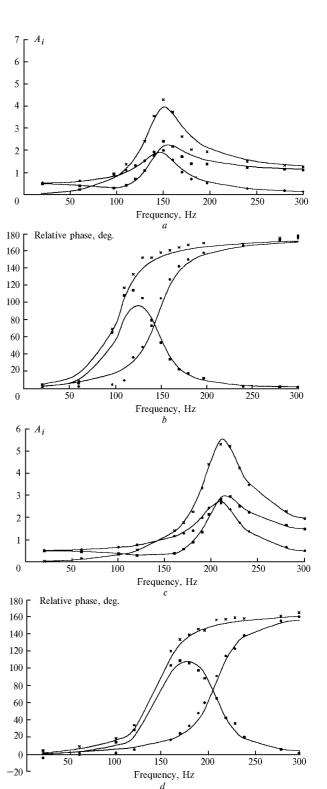
Fig. 7. Frequency characteristics (relative amplitude and phase difference) of the HR and DHR configurations with one (a, b) and two (c, d) capillary tubes, respectively. U_1/U_0, $\varphi_1 - \varphi_0$ (squares); U_2/U_0, $\varphi_0 - \varphi_2$ (HR) (circles), and $(U_1 - U_0)/U_0$, $\varphi_1 - \varphi_2$ (DHR) ($\times$) are the mean experimental values for various C_2H_4:N_2 mixtures. The solid curves are for the frequency characteristics of the equivalent electrical circuits shown in Fig. 4b and c.
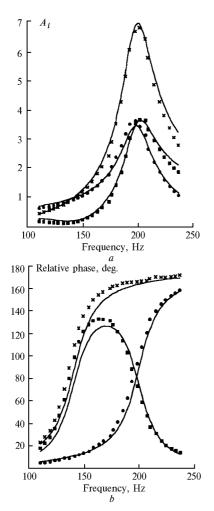
Fig. 8. Frequency characteristics of HR and DHR with one and two capillary tubes. The cells are filled with pure C_2H_4 at the pressure of 1 atm. Notations are the same as in Fig. 7.

Fig. 9. Frequency characteristics of HR and DHR with two capillary tubes at the pressure in the cell: 0.5 atm (C_2H_4:N_2 = 1:4) (*a*) and 0.1 atm (pure C_2H_4) (*b*). Notations are the same as in Fig. 7.

At the atmospheric pressure, pressure broadening of spectral lines substantially restricts the spectral selectivity of the pollution monitoring, especially, in the spectral ranges, where significant absorption by principal atmospheric gases, like water vapor and CO_2, takes place. At the reduced pressure the line width decreases proportionally to P^{-1}, and it becomes possible to distinguish the absorption lines of pollutants from those of main gaseous constituents of the atmosphere. At the pressure ranging from 1000 to 100 mbar, the decrease in the density of the measured gas is compensated for by narrowing of the spectral line, and the absorption coefficient in the line center decreases only by about 30%. The threshold sensitivity of a PA spectrometer (gas analyzer) at the reduced pressure is determined only by the properties of acoustic resonator (as shown above, R_{C0} remains unchanged and R_m increases as the pressure falls). The frequency characteristics of HR and DHR at the reduced pressure are shown in Fig. 9. At low pressure (100 mbar) the Helmholtz resonance is observed, and the ratio A_{12} is nearly three; the value of resonance frequency therewith is pressure independent.
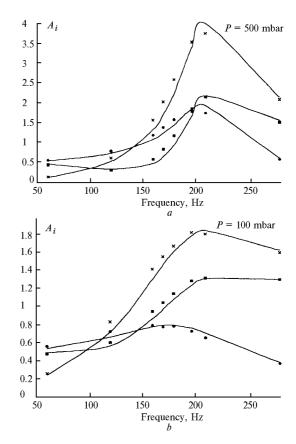
At the resonance frequency, the gas in the capillary tube connecting two identical volumes of the PA cell moves like a piston compressing the gas in one volume while expanding it in another. The PA signals from the two volumes are therefore opposite in phase (Figs. 7, 8, 10, and 11). In Ref. 14 this fact was used to double the signal amplitude and to fully suppress the cophased noise by recording the difference of signals from the microphones in the cells.

However, the fact that the PA signals (namely, pressure oscillations) in different cells are opposite in phase for the first time gave us the possibility to use the part of the laser power, lost on the chopper disk of the standard chopper, for enhancement of the PA signal. Using a mirror sector disk instead of the standard one and a beam-turning mirror, we have exposed both the PA cells to the modulated radiation exactly opposite in phase and have obtained doubling of the ratios A_1, A_2, and A_{12} at the resonance frequency. This actually, according to Eq. (22), corresponds to doubling of the sensitivity R. Setting of an additional heat source into the second cell corresponds to including an additional current source connected to the second capacitor into the equivalent electrical circuit (Fig. 4*b*). The proposed model also describes the frequency characteristics of the resonators with the
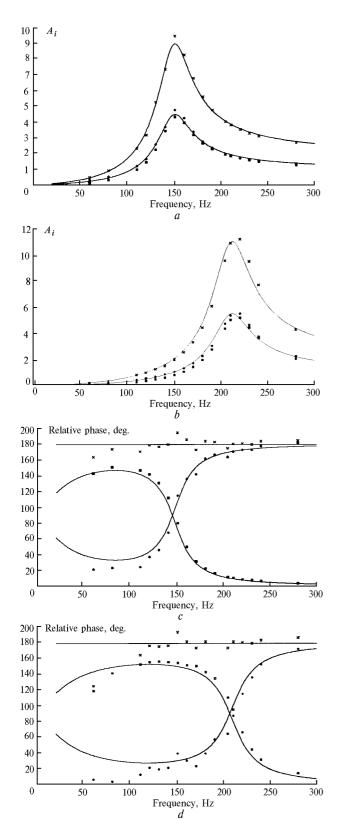
Fig. 10. Frequency characteristics of HR and DHR with one (*a*, *c*) and two (*b*, *d*) capillary tubes. The cells of the PA detector are exposed to radiation in antiphase with the use of the mirror chopper. The cells are filled with $C_2H_4{:}N_2 =$ = 1.7/1000 at the pressure of 1 atm. Notations are the same as in Fig. 7.

experimental accuracy (Fig. 10); the ratios A_1 and A_2 therewith are equivalent and equal to zero for frequencies lower than the resonance one, and the phase shifts are equal to π in the whole frequency region.

The processes of adsorption and desorption of the gas on cell walls significantly change its concentration in a closed volume. To eliminate the influence of these processes on the measurement accuracy, flow measurements are carried out thus leading to the substantial (one to three orders of magnitude) enhancement of ambient acoustic noise. Therefore, to decrease the noise, a rather sophisticated design of the PA cells is required.[1,2,7,8]
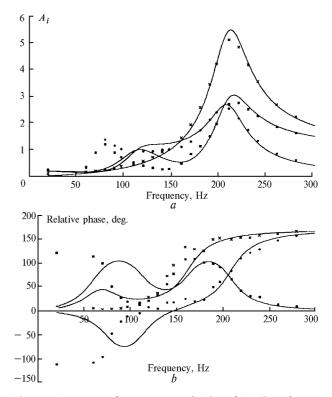

Fig. 11. Frequency characteristics of HR and DHR with two capillary tubes at flow measurements. Notations are the same as in Fig. 7. The equivalent electrical circuit is shown in Fig. *4d*.

The DHR configuration of the PA cells gives an opportunity to carry out flow measurements. The design of our PA system has a bilateral symmetry. The cell volumes through which the gas is passed are identical, so the pressure oscillations due to gas flows in the cells are almost matched in phase, and they are subtracted, as well as the ambient acoustic noise. The scheme of the PA detector intended for flow measurements and the equivalent electrical circuit are shown in Fig. *4d*. The additional discrete elements of the electrical circuit L_a, R_a, and C_a correspond to the part of the capillary tube (Fig. *1c*) and the additional volume of the interconnecting vacuum tube (6 mm in diameter and 1.1 m in length). The experimental values and frequency characteristics of the equivalent circuit for

HR coincide in the region of the fundamental resonance and have different additional resonances in the region of low modulation frequencies (Fig. 11). Note that the experimental values in this case are lower than the predicted ones. The dimensions of the additional volume (length of 1.1 m) are comparable with the acoustic wavelength (about 3.5 m), therefore the models of equivalent electrical circuits with distributed parameters should be used in this case.[12,13] In the case of DHR, the experimental and calculated frequency characteristics have no additional resonances due to phase matching of the HR signals in the region of low frequencies. Figure 12 shows the reduction of the noise level in the DHR configuration as compared to the nonresonant detector for the flow measurements (the room air flow rate is about $2 \cdot 10^{-5}$ m$^3 \cdot$s^{-1}).
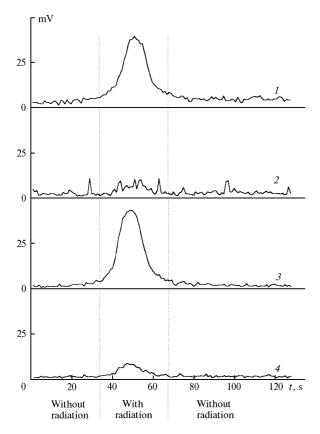

Fig. 12. Noise suppression in DHR at flow measurements: DHR cell for flow operation (*1*); nonresonant PA cell for flow operation (*2*); DHR cell for flowless operation (*3*); nonresonant PA cell for flowless operation (*4*).

7. Conclusion

The testing of the DHR configuration of the PA detector has demonstrated its advantages and prospects in application to both laser gas analyzers and spectroscopy of weakly absorbing gases. Relatively simple design of the DHR cell together with the mirror chopper instead of the standard mechanical chopper provides the ability to double the amplitude of the

valid signal and increase the S/N ratio by an order of magnitude. This construction of the PAD allows designing small-size spectrometers–gas-analyzers based on low-power diode lasers for flow measurements. In Ref. 35 we have reported on efficient applicability of the DHR detector for investigation into transformation of the absorption line contour of methane by buffer gas pressure with the use of the diode laser (output power of 1 mW) operating at the room temperature as an emission source. The threshold sensitivity to the methane concentration was 60 ppm in that case.

Table 2. Specifications of DHR with two capillary tubes

Length of the PA cell, mm	102
Cell diameter, mm	10.8
Length of the capillary tube, mm	83
Diameter of the capillary tube, mm	2.06
Resonance frequency f_R, Hz	210
Q-factor Q	5.4
Microphone sensitivity R_m at the frequency of 210 Hz, Pa^{-1}	10
DHR sensitivity R_C, Pa$\cdot$W$^{-1}\cdot$cm	6600
Level of acoustic noise, μV$\cdot$Hz$^{-1/2}$	1
Threshold sensitivity to absorption, W$\cdot$cm^{-1}	$1.5 \cdot 10^{-8}$
Detection limit for the absorption coefficient with the use of diode laser with output power of 0.7 mW, cm^{-1}	$2 \cdot 10^{-5}$
Detection limit for CH$_4$ concentration with the use of diode laser operating at 1.65 μm with output power of 0.7 mW, ppm	~ 60

For theoretical description of the characteristics of the open-type DHR cells, we have refined and supplemented the equations describing generation of an acoustic signal, in particular, properly took into account the relaxation of excited molecules on the cell walls. This allowed us to achieve very good agreement between the calculated and experimental data within the experimental accuracy for the dependence of the sensitivity of a PA cell on its geometry, gas pressure, and modulated frequency of the exciting radiation.

Finally, we have checked the method of electroacoustic analogy with discrete parameters of electrical circuits for its efficiency in studying the Helmholtz acoustic resonators of various configurations.

References

1. P.L. Meyer and M.W. Sigrist, Rev. Sci. Instrum. **61**, 1779 (1990).

2. A. Thony and M.W. Sigrist, Infrared Phys. Technol. **36**, 585 (1995).

3. M. Feher, Y. Jiang, J.P. Maier, and A. Miklos, Appl. Opt. **33**, 1655 (1994).

4. F.J.M. Harren, F.J.C. Bijnen, J. Reuss, L.A.C.J. Voesenec, and C.W.P.M. Blom, Appl. Phys. B: Photophys. and Laser Chem. **50**, 137 (1990).

5. R.A. Rooth, A.J.L. Verhage, and L.W. Wouters, Appl. Opt. **29**, 3643 (1990).

6. J. Henningsen, T. Migelberg, and M. Hammerich, J. de Phys. IV **4**, 499 (1994).

7. G.Z. Angeli, Z. Bozoki, A. Miklos, A. Lorincz, A. Thony, and M.W. Sigrist, Rev. of Sci. Instrum. **62**, 810 (1991).

8. R.S. Quimby, P.M. Selzer, and W.M. Yen, Appl. Opt. **16**, 2630 (1977).

9. N.C. Fernelius, Appl. Opt. **18**, 1784 (1979).

10. W.A. McClenny, C.A. Bennett Jr., G.M. Russwurm, and R. Richmond, Appl. Opt. **20**, 650 (1981).

11. O. Nordhaus and J. Pelzl, Appl. Phys. **25**, 221 (1981).

12. J. Pelzl, K. Klein, and O. Nordhaus, Appl. Opt. **21**, 94 (1982).

13. R. Kastle and M.W. Sigrist, Appl. Phys. **B63**, 389 (1996).

14. G. Busse and D. Herboeck, Appl. Opt. **18**, 3959 (1979).

15. D. Pereira and A. Scalabrin, Infrared Phys. **33**, 549 (1992).

16. E.L. Kerr and J.G. Atwood, Appl. Opt. **7**, 915 (1968).

17. L.B. Kreuzer, J. Appl. Phys. **42**, 2934 (1971).

18. L.G. Rosengren, Infrared Phys. **13**, 109 (1973).

19. E. Max and L.G. Rosengren, Opt. Commun. **11**, 422 (1974).

20. L.G. Rosengren, Appl. Opt. **14**, 1960 (1975).

21. A.B. Antipov, V.A. Kapitanov, Yu.N. Ponomarev, and V.A. Sapohznikova, *Optoacoustic Method in Laser Spectroscopy of Molecular Gases* (Nauka, Novosibirsk, 1984), 128 pp.

22. D.R.Lide, ed., *Handbook of Chemistry and Physics,* 72nd edn (CRC Press, Boston, 1991−1992).

23. Jr.C.F. Dewey, Opt. Eng. **13**, 483 (1974).

24. C.K.N. Patel and R.J. Kerl, Appl. Phys. Lett. **30**, 578 (1977).

25. A. Miklos, Z. Bozoki, Y. Jiang, and M. Feher, Appl. Phys. B: Lasers and Opt. **58**, 483 (1994).

26. V.A. Kapitanov, Yu.N. Ponomarev, D. Courtois, V. Zeninari, Infrared Phys. Technol. **40**, 1 (1999).

27. V.P. Zharov and V.S. Letokhov, *Laser Optoacoustic Spectroscopy* (Springer−Verlag, Berlin, 1986), 280 pp.

28. K. Stephan, V. Rothacker, and W. Hurdelbrink, Chem. Eng. Process. **26**, 257 (1989).

29. K. Stephan and J. Biermann, Intern. J. Heat Mass Transfer **35**, 605 (1992).

30. M. Margottin-Maclou, L. Doyennette, and L. Henry, Appl. Opt. **10**, 1768 (1971).

31. L.C. Aamodt and J.C. Murphy, J. Appl. Phys. **48**, 927 (1977).

32. Knowles Electronics Co., 73 Victoria Road, Burgess Hill, RH15 9LP, UK.

33. L.G. Parker and D.N. Ritke, J. Chem. Phys. **59**, 3713 (1973).

34. M.A. Sapozhkov, *Electroacoustics* (Svyaz', Moscow, 1978), 272 pp.

35. V.A. Kapitanov, Yu.N. Ponomarev, D. Courtois, and V. Zeninari, in: *Abstracts of Reports at the 13-th International Symposium and School on High Resolution Molecular Spectroscopy*, Tomsk (1999), p. 22.